HHS Public Access

Author manuscript

Nat Med. Author manuscript; available in PMC 2015 April 01.

Published in final edited form as:

Nat Med. 2014 October ; 20(10): 1187–1192. doi:10.1038/nm.3611.

An Intracellular Ca^{2+} Channel is Required For Sarcolemma Repair to Prevent Muscular Dystrophy

Xiping Cheng[1,*], **Xiaoli Zhang**[1], **Qiong Gao**[1], **Mohammad Ali Samie**[1], **Marlene Azar**[1], **Wai Lok Tsang**[1], **Libing Dong**[1], **Nirakar Sahoo**[1], **Xinran Li**[1], **Yue Zhuo**[1], **Abigail G. Garrity**[1,2], **Xiang Wang**[1], **Marc Ferrer**[3], **James Dowling**[4,5], **Li Xu**[6], **Renzhi Han**[6], and **Haoxing Xu**[1,2,*]

[1]Department of Molecular, Cellular, and Developmental Biology, University of Michigan, 3089 Natural Science Building (Kraus), 830 North University, Ann Arbor, MI 48109, USA

[2]Neuroscience Graduate Program, University of Michigan, Ann Arbor, MI 48109, USA

[3]NIH/NCATS/NCGC, 9800 Medical Center Drive, Rockville, MD 20850, USA

[4]Department of Pediatrics, University of Michigan Medical Center, Ann Arbor, MI 48109, USA

[5]Division of Neurology and Program of Genetics and Genome Biology, Hospital for Sick Children, Departments of Pediatrics and Molecular Genetics, University of Toronto, Toronto, ON M5G 0A4, Canada

[6]Department of Cell and Molecular Physiology, Loyola University Chicago Health Sciences Division, IL 60153, USA

Abstract

The integrity of the plasma membrane is maintained through an active repair process, especially for skeletal and cardiac muscle cells, in which contraction-induced mechanical damage frequently occurs *in vivo*[1,2]. Muscular dystrophies (MDs) are a group of muscle diseases characterized by skeletal muscle wasting and weakness[3,4]. An important cause of MD is defective repair of sarcolemmal injuries, and sarcolemma repair requires Ca^{2+} sensor proteins[5–8] and Ca^{2+}-dependent delivery of intracellular vesicles to injury sites[5,8,9]. TRPML1 (ML1) is an endosomal and lysosomal Ca^{2+} channel and its human mutations cause Mucolipidosis IV, a neurodegenerative disease with motor disabilities[10,11]. Here, we report that ML1-null mice develop a primary, early-onset muscular dystrophy independent of neural degeneration. Although the dystrophin-glycoprotein complex and the known membrane repair proteins are normally expressed, membrane resealing was defective in ML1-null muscle fibers or upon acute and pharmacological inhibition of ML1 channel activity or vesicular Ca^{2+} release. Injury facilitated the trafficking and

Correspondence should be addressed to H.X. (haoxingx@umich.edu) or X.C. (xpcheng@umich.edu).

The authors have no competing interests as defined by Nature Publishing Group, or other interests that might be perceived to influence the results and/or discussion reported in this paper.

Author contribution:

X.C. initiated the project; H.X., X.C., J.D. and R.H. designed the research; X.C., X.Z., Q.G., M.A.S., M.A., W.L.T. and L.D. performed the research; N.S., X.L., A.G.G., X.W., M.F. and L.X. contributed the new regents; X.C., X.Z, Q.G., M.A.S., M.A., W.L.T., J.D., R.H. and H.X. analyzed the data; and H.X. and X.C. wrote the paper with inputs from all the authors.

exocytosis of vesicles by upmodulating ML1 channel activity. In the dystrophic mdx mouse model, overexpression of ML1 decreased muscle pathology. Collectively, we have identified an intracellular Ca^{2+} channel that regulates membrane repair in skeletal muscle via Ca^{2+}-dependent vesicle exocytosis.

Keywords

Membrane repair; Ca^{2+}; TRP channel; lysosome

A mouse model with targeted deletion of the *ML1* gene (ML1 knockout or KO; $ML1^{-/-}$)[11] was confirmed by PCR genotyping (Supplementary Fig. 1a). In skeletal muscle and cultured myoblasts isolated from ML1 KO mice, reverse transcription-PCR analysis could not detect full-length ML1 transcript (Fig. 1a). Consistently, patch-clamping of the endolysosomal membranes[12] showed that whole-endolysosome ML1-like currents (I_{ML1}) were activated by ML-SA1, a membrane-permeable TRPML-specific synthetic agonist[13] in WT but not ML1 KO primary cultured myoblasts (Fig. 1b). I_{ML1} was potently inhibited by ML-SI compounds (Fig. 1b), which are membrane-permeable TRPML-specific synthetic antagonists[14].

At 1 month of age, ML1 KO mice are grossly healthy and do not exhibit any obvious neurodegeneration[11]. However, when they are challenged with a 15° downhill treadmill test at the speed of 20 m/min, ML1 KO mice show a pronounced defect in their motor abilities and a greatly reduced treadmill staying time (Fig. 1c). Histological analysis of various tissues involved in the movement impairment revealed, unexpectedly, that the skeletal muscles of ML1 KO mice exhibited clear signs of dystrophy even at 1 month (Fig. 1d,e). By 1 month, individual necrotic and centrally nucleated fibers were detectable in $ML1^{-/-}$ skeletal muscle (Fig. 1d,e). In contrast, no obvious dystrophy was seen in WT skeletal muscle (Fig. 1e,f). By three months, central nucleation, fibrosis (fibrous scar tissue and fat replacement), and immune cell infiltration were commonly seen (Fig. 1d,e & Supplementary Fig. 1). As observed in most animal models of MD[15], the distribution of the dystrophic area in skeletal muscle was heterogeneous. For example, for the Gastroctrocnemius (Gastroc) muscle, the dystrophic area was mainly concentrated on the periphery of the muscle and the central region remained largely intact (Fig. 1d). A characteristic of MD is muscle regeneration triggered by degeneration, forming a cycle of degeneration and regeneration[4,9]. Hence, centrally nucleated muscle fibers and smaller-sized fibers are frequently observed, which reflects muscles undergoing active regeneration[4,9]. Consistent with this finding, $ML1^{-/-}$ fibers were relatively small in size and with a high degree of central nucleation (Fig. 1d, g, h).

ML1 KO mice exhibited progressive MD, with severity increasing with age (Fig. 1e–g). Muscle-specific heterogeneity is commonly seen in MD, potentially due to the variability in their use-dependent physical activity[3,4]. At 1 month old, only about half of the skeletal muscles, including the triceps, quadriceps, hamstring, and Gastroc muscles, manifested dystrophy (Supplementary Fig. 1c). In contrast, the diaphragm, iliopsoas, gluteus, soleus, and tibialis anterior muscles appeared normal (Supplementary Fig. 1c). However, at 3 months, more skeletal muscles developed dystrophy (Supplementary Fig. 1d). Both type 1

slow-twitch and type 2 fast-twitch muscle fibers were dystrophic (Supplementary Fig. 2a). However, cardiac and smooth muscles did not exhibit obvious pathology (Supplementary Fig. 2b). These results suggest that ML1-null mice exhibited early-onset, progressive, and extensive MD.

Evans blue (EB) dye is a reliable *in vivo* marker of myofiber damage[16]. A small but significant percentage of ML1-null Gastroc myofibers were EB-positive at rest (Fig. 2a,b). After a 15° downhill treadmill exercise, the percentage of EB-positive cells in the ML1-null Gastroc muscle increased from 2% to 12% (Fig. 2a,b). In comparison, the percentage of EB-positive cells in WT littermates never exceeded 1%, even after treadmill exercise (Fig. 2a,b). Another measure of myofiber damage is the leakage of muscle proteins to the serum[3,4]. Consistent with the EB analysis, the serum creatine kinase (CK) levels of ML1-null mice were 2–3-fold higher than those of WT littermates (Fig. 2c). Treadmill exercise further increased serum CK levels (Fig. 2c). Taken together, these results suggest that an increase in muscle membrane damage underlies MD in ML1 KO.

Although muscle pathology and elevated CK levels were initially reported in some ML4 patients[17,18], ML4 has generally been considered a disease of neural degeneration[10,11], which could explain the motor defects of ML4 patients and ML1 KO mice. Consistent with previous reports[11,19], ML1 KO mice did exhibit neuronal cell death, but only at ages >5 months (Supplementary Fig. 2c). At younger ages (1–3 months) motor neurons in the spinal cord did not show any obvious sign of neural degeneration (Supplementary Fig. 1d). Likewise, sciatic nerve myelination was normal in ML1 KOs at one month (Fig. 2d). Furthermore, in conditions mimicking neural degeneration, such as sciatic nerve axotomy, no dystrophic phenotype was observed (Fig. 2e). Instead, axotomy resulted in muscle atrophy, which manifested as a homogeneous decrease in fiber size (Fig. 2e). In addition, Gastroc muscle from the mouse model of Fabry's disease[20] exhibited denervation-like effects on the fiber size, without exhibiting MD-like necrosis and central nucleation (Fig. 2f). In 1-month-old ML1-null mice, lysosome storage was barely observed in the dystrophic muscles (Supplementary Fig. 2e). Collectively, muscle dystrophy in the ML1-null mice is unlikely to be a secondary effect of neural degeneration or a lysosome storage defect.

To directly investigate the dystrophic mechanisms caused by ML1 deficiency, we performed a rescue experiment involving intramuscular injection of an adeno-associated virus (AAV) carrying the GFP-ML1 transgene (AAV-GFP-ML1), which typically infected the majority (>85%) of the muscle fibers. As was observed in many LSDs, ML1-null muscle exhibited a compensatory increase in the key lysosomal protein Lamp1[13], as shown by Lamp1 immunofluorescence staining and western blot analysis (Supplementary Fig. 3a,b). However, when compared with the adjacent noninfected and contralateral uninfected muscle fibers, ML1-null Gastroc muscle infected with AAV-GFP-ML1 (localized in Lamp1-positive compartments; see Supplementary Fig. 3c,d) experienced a dramatic AAV-infection mediated decrease of elevated Lamp1 expression (Fig. 2g & Supplementary Fig. 3e). AAV-ML1-GFP infection reduced the dystrophic area (Fig. 2h), collagen content (Fig. 2i), and the percentage of EB-positive muscle fibers (Fig. 2j). Hence, expression of ML1 in muscle was sufficient to rescue the MD of ML1 KO, suggesting a cell-autonomous mechanism as the underlying cause of MD.

Mechanical stress can cause myofiber necrosis by two separate mechanisms. First, the sarcolemma of a muscle fiber could be more susceptible to damage, as seen in the dystrophin (a core component of DGC) mutant (mdx) mice[4,21]. Second, a muscle fiber could have a defect in sarcolemma repair, as seen in dysferlin or MG53 KO mice[5,9,22]. The majority of human MD mutations are linked to defects in the components of the DGC[4]. However, no obvious decrease in expression was observed for any of core and accessory components of the DGC being examined, which included dystrophin, β-DG, integrin β1, and laminin (Fig. 3a,b). Furthermore, the expression of dysferlin, cav-3, and MG53, three proteins known to be involved in sarcolemma repair and human MD[4,5,23], also exhibited no decrease in ML1-null muscle (Fig. 3a,b).

To create plasma membrane disruptions and to evaluate the resealing efficiency, single myofibers isolated from the flexor digitorum brevis (FDB) muscle were irradiated with a two-photon laser[5,9]. FM1–43, a membrane-impermeable fluorescent dye that preferentially adheres to lipids, is commonly used to detect membrane disruptions[5]. Rapid FM dye entry and accumulation were observed within seconds after laser irradiation (Fig. 3c & Supplementary Fig. 4a). However, in WT muscle fibers, dye entry ceased shortly (1–2 min) after irradiation, suggesting successful membrane resealing (Fig. 3c). In contrast, upon identical laser irritation, ML1-null fibers continued FM dye uptake at the injury sites for several minutes (Fig. 3c), suggesting failed membrane resealing. Removal of extracellular Ca^{2+} caused rapid accumulation of FM dyes at the injury sites indistinguishably for WT or ML1-null myofibers (Supplementary Fig. 4b). Defective membrane resealing was also observed in ML1-null myotubes that were exposed to mechanical damage elicited by microelectrode penetration into the sarcolemmal membrane (Fig. 3d). Unlikely most WT myotubes, the majority (>80%) of ML1-null myotubes were not able to “survive” the prolonged contractions caused by continuous Ca^{2+} entry (see below).

Next, pharmacological experiments were performed on C2C12-derived myotubes with the microelectrode penetration assay[24]. No significant FM4–64 dye was seen at injury sites, even with repeated penetrations (Fig. 3e). In contrast, removal of extracellular Ca^{2+} significantly increased the entry of FM dyes (Supplementary Fig. 4c), suggesting that the influx of extracellular Ca^{2+} is essential for repair[8]. In the presence of BAPTA-AM to chelate intracellular Ca^{2+} or glycyl-L-phenylalanine 2-naphthylamide (GPN), a lysosome-targeted cathepsin C substrate, to specifically deplete the lysosomal Ca^{2+} store[13], significant dye entry was observed even under normal extracellular Ca^{2+} concentrations (2 mM; Fig. 3e). These results suggest that lysosomal Ca^{2+} also has a role in membrane resealing. To monitor the Ca^{2+} levels at injury sites, myoblasts and C2C12 cells were transfected with Lamp1-GCaMP3, a lysosome-targeted genetically encoded Ca^{2+} indicator[13]. Transient Ca^{2+} increases were observed at injury sites in the presence or absence of external Ca^{2+} (Supplementary Fig. 4d–g). However, intracellular Ca^{2+} release was less in ML1 KO myoblasts or in the presence of ML-SI compounds[25] (Supplementary Fig. 4f, g), suggesting a contribution to Ca^{2+} release from lysosomes during membrane damage or early stage of membrane repair. In the presence of external Ca^{2+}, prolonged Ca^{2+} influx was observed in ML1 KO myoblasts or ML-SI3-treated C2C12 myoblasts (Supplementary Fig. 4d, e). Hence, ML1 plays a dual role in promoting the initial phase of Ca^{2+} increase (within seconds) but inhibiting the prolonged phase of Ca^{2+} increase (lasting minutes).

To test whether ML1 plays a direct role in membrane repair, we acutely inhibited ML1 channel function using ML-SIs. Notably, in experiments performed by researchers who were blind to experimental conditions, significant FM4–64 dye uptake was seen in the presence of three structurally independent ML-SI compounds (Fig. 3e & Supplementary Fig. 4c). We also employed ML1 inhibitors to test the role of ML1 in sarcolemma repair *in vivo*. Cardiotoxin VII4 (CTX) is a toxin that can induce membrane damage *in vivo* to cause EB dye accumulation in muscle cells[24]. EB-positive muscle cells were more numerous in CTX-treated ML1-null muscle than in CTX-treated WT controls (Supplementary Fig. 4h). Notably, co-injection of ML-SI3 with CTX markedly increased the percentage of EB-positive muscles in CTX-treated WT mice, to the same level as that of CTX-treated ML1-null mice (Fig. 3f & Supplementary Fig. 4h).

Chemical injuries from streptolysin O (SLO) toxin is commonly employed to induce membrane repair responses, and propidium iodide (PI) staining is a common readout for membrane damage and cell viability[26]. In non-muscle cells, including mouse embryonic fibroblasts (MEFs) and bone marrow-derived macrophages (BMMs), SLO treatment caused more PI-positive cells for ML1 KO (Fig. 4a & Supplementary Fig. 5). In addition, ML-SI3 increased PI staining in WT, but not KO cells (Fig. 4a & Supplementary Fig. 5). Conversely, ML1 overexpression decreased PI staining (Supplementary Fig. 5). These results suggest that ML1 may be a core component of the membrane repair machinery in both muscle and non-muscle cells.

Membrane resealing requires the fusion and exocytosis of intracellular vesicles at sarcolemma injury sites[8]. Upon SLO treatment, pHluorin TIRF imaging[27] showed that ML1 and Vamp7 doubly-positive vesicles underwent exocytosis (Supplementary Fig. 6a & Video 1). Exocytosis of ML1-resident vesicles may lead to the appearance of ML1 proteins at the plasma membrane. Hence, measurement of whole-cell ML1 currents may provide a readout for exocytosis[14]. Consistently, SLO treatment also increased whole-cell I_{ML1} by 2–3-fold in C2C12 cells (Fig. 4b, c). ML-SI3-mediated inhibition of ML1 and ML1 KO, on the other hand, significantly reduced SLO-induced lysosomal exocytosis as measured by Lamp1 surface staining[28] (Supplementary Fig. 6b,c) and lysosomal enzyme (AP or acid SMase[29]) release (Fig. 4d, e) in muscle cells and MEFs. Collectively, these results suggest ML1-mediated lysosomal exocytosis may play an important role in membrane resealing.

Consistent with the possibility that overexpression of ML1 promotes membrane repair in mdx muscle[4,21], AAV-GFP-ML1-infected muscle exhibited a significant reduction in both EB dye uptake and dystrophic area compared with the contralateral noninjected control muscle (Fig. 4f, g).

ML1-null mice exhibit a primary early-onset MD that is caused by defective membrane resealing. Similar but less dramatic dystrophic phenotype was observed in mice lack MG53 or dysferlin, two proteins known to be involved in membrane repair[5,9]. By interacting with Ca^{2+} sensors in the vesicles, for example, dysferlin and Syt-VII[5,6], ML1 may mediate membrane repair by promoting vesicle exocytosis in both muscle and non-muscle cells (Supplementary Fig. 7). The initial rapid Ca^{2+} increase, within 10–20 seconds, is essential for triggering the resealing process. Depending on the nature of the damage and size of the

wound, three different mechanisms may be employed for membrane repair: membrane patching, endocytosis, and shedding[8,29,30]. Previous studies have unequivocally established the roles of extracellular Ca^{2+} in all *in vitro* assays and models of membrane repair[5,28,30]. We show in the current study that lysosomal Ca^{2+} is also essential for this process, even in the presence of extracellular Ca^{2+}, suggesting an involvement of more than one Ca^{2+} source. Consistently, multiple Ca^{2+} sensors are implicated in sarcolemma repair, including dysferlin, myoferlin, annexin, Syt-VII, Alix/ALG-2, and calcineurin[8,30]. Although lysosomes have long been implicated in membrane repair in non-muscle cells[28], their role in sarcolemma repair has remained unclear. Notably, the expression level of the housekeeping lysosomal protein Lamp1 that is compensatorily upregulated in many LSDs is also elevated in dysferlin-null mice[31]. In addition, mice lacking Syt-VII, a lysosome-specific Ca^{2+} sensor, exhibit a MD-like phenotype[6]. Hence, the sarcolemma repair system may have a close relationship with the late endocytic pathway.

ONLINE METHODS

Reverse transcription-PCR

Total RNA was extracted from muscle tissues or cultured myoblasts and dissolved in TRIzol (Invitrogen). First-strand cDNA, synthesized with Superscript III RT (Invitrogen), was used for reverse transcription-PCR analysis of ML1 expression based on the following intron-spanning primer pair (and L32 control):

Forward: AAACACCCCA GTGTCTCCAG; Reverse: GAATGACACC GACCCAGACT

L32: Forward: TGGTGAAGCC CAAGATCGTC; Reverse: CTTCTCCGCA CCCTGTTGTC

Plasmid construction

Generation of the plasmids used in this study (GFP-ML1, mCherry-ML1, CFP-ML1, GCaMP3-ML1, Lamp1-GCaMP3, and Vamp7-pHluorin) was reported previously[13,27].

Western blot and immunoprecipitation

Standard western blotting protocol was used. Gastroctrocnemius muscle was lysed with ice-cold RIPA buffer in the presence of 1X protease inhibitor cocktail (Sigma). For each sample, 10 μg to 100 μg of total protein was loaded onto 4–12% SDS-polyacrylamide gradient gels (Invitrogen), and transferred to PVDF membranes. The membranes were blocked for 1 h with 1% BSA in PBST and incubated with various antibodies against dystrophin (Abcam), β-dystroglycan (β-DG) (Santa Cruz), caveolin-3 (BD Biosciences), dysferlin (Abcam), myosin (Iowa Hybridoma Bank), MG53 (Novus Biologicals), and Lamp1 (ID4B; Iowa Hybridoma Bank) in PBST. The blots were detected by using Peroxidase-conjugated anti-rabbit/mouse/rat secondary antibody with an enhanced chemiluminescence reagent (Amersham Pharmacia Biotech).

Mouse lines

The generation and characterization of ML1 KO mice (in a B6:129 mixed genetic background) were described previously[11,14]. Mdx mice were ordered from Jackson Laboratories. Fabry's mice[32] were a gift from Dr. James Shayman. Mice were used under approved animal protocols and Institutional Animal Care Guidelines at the University of Michigan. Littermates were used as controls in the mouse experiments. Mice were randomly assigned to both control and testing groups, each typically contain 3–5 animals.

Treadmill exercise

Mice were trained to run on an Exer-6M treadmill (Columbus Instruments) with a 15° downhill angle at the speed of 12–20 m/min.

Muscle cell culture

Murine myoblasts were prepared and cultured as described previously[33]. Briefly, limb muscles were isolated and dissociated with 1% collagenase and 0.25% trypsin treatment at 37 °C. After pre-plating on a standard Petri dish (non-tissue culture-coated) for 60–90 min to remove fibroblasts, muscle cells were maintained at 37 °C and 5% CO_2 in F10 medium with 20% FBS (Gibco). To induce differentiation, myoblasts were grown to confluence before switching to DMEM containing 5% horse serum. For transient transfections, myoblasts were plated at 70% confluence and transfected by using Lipofectamine 2000 reagent (Invitrogen). Live cell imaging experiments were performed 24–48 h after transfection or at the times indicated for individual experiments.

The myogenic C2C12 murine myoblast cell line was purchased from the American Type Culture Collection (Manassas, VA). Cells were grown in a humidified environment at 37 °C and 5% CO2 in DMEM medium supplemented with 20% FBS and penicillin (100 units/ml) and streptomycin (100 μg/ml). C2C12 cell differentiation was induced by switching to DMEM medium containing 5% horse serum.

Fluorescence and time-lapse confocal imaging

Live imaging of C2C12 or primary myoblasts was performed on a heated stage on a spinning disk confocal imaging system, which consisted of an Olympus IX81 inverted microscope, a 60X or 100X objective (Olympus), a CSU-X1 scanner (Yokogawa), an iXon EM-CCD camera (Andor), and MetaMorph Advanced Imaging acquisition software v. 7.7.8.0 (Molecular Devices). For immunofluorescence detection, cells or muscle sections were fixed with 4% PFA, permeabilized with 0.03% Triton X-100, and stained with various primary antibodies: EEA1 (Abcam), Lamp1 (ID4B), dystrophin, β-DG, integrin β1 (Iowa Hybridoma Bank), and laminin (Chemicon).

Whole-endolysosome electrophysiology

Endolysosomal electrophysiology was performed on isolated endolysosomes with a patch clamp method as described previously[12,34]. Briefly, cells were treated with 1 μM vacuolin-1 for 2–5 h to increase the size of endosomes and lysosomes. Whole-endolysosome recordings were performed on isolated enlarged endolysosomes. The bath (internal/cytoplasmic)

solution contained 140 mM K-gluconate, 4 mM NaCl, 1 mM EGTA, 2 mM Na_2-ATP, 2 mM $MgCl_2$, 0.39 mM $CaCl_2$, 0.2 mM GTP, and 10 mM HEPES [pH adjusted with KOH to 7.2; the free $[Ca^{2+}]_i$ was estimated to be ~100 nM on Maxchelator software (http://maxchelator.stanford.edu/)]. The pipette (luminal) solution consisted of a 'low pH Tyrode's solution' with 145 mM NaCl, 5 mM KCl, 2 mM $CaCl_2$, 1 mM $MgCl_2$, 10 mM HEPES, 10 mM MES, and 10 mM glucose (pH 4.6). All bath solutions were applied via a perfusion system to achieve a complete solution exchange within a few seconds. Data were collected with an Axopatch 2A patch clamp amplifier, Digidata 1440, and pClamp 10.0 software (Axon Instruments). Currents were digitized at 10 kHz and filtered at 2 kHz. All experiments were conducted at room temperature (21–23 °C), and all recordings were analyzed with pClamp 10.0 and Origin 8.0 (OriginLab, Northampton, MA, USA).

Whole-cell electrophysiology

Whole-cell recordings were performed as described previously[13,35]. The pipette solution contained 147 mM Cs, 120 mM methane sulfonate, 4 mM NaCl, 10 mM EGTA, 2 mM Na_2-ATP, 2 mM $MgCl_2$, and 20 mM HEPES (pH 7.2; free $[Ca^{2+}]_i$ < 10 nM). The standard extracellular bath solution (modified Tyrode's solution) contained 153 mM NaCl, 5 mM KCl, 2 mM $CaCl_2$, 1 mM $MgCl_2$, 20 mM HEPES, and 10 mM glucose (pH 7.4).

GCaMP3 Ca^{2+} imaging

GCaMP3 Ca^{2+} imaging was performed in primary myoblasts or C2C12 cells that were transfected with Lamp1-GCaMP3 and GCaMP3-ML1, which are lysosome-targeted genetically encoded Ca^{2+} sensors[13]. The fluorescence intensity at 488 nm (F_{488}) was recorded with the spinning disk confocal imaging system.

H&E and histochemical staining

H&E staining was performed in 12-μm-thick sections that were prepared from freshly frozen tissues and fixed with 4% PFA. Myosin ATPase staining was performed at pH 4.3; at this pH, type 1 slow-twitch fibers are dark-colored and type 2 fast-twitch fibers are light-colored[36].

Collagen content measurement

The level of hydroxylproline, a major component of collagen[6], was measured using Hydroxyproline Assay Kit (Sigma).

Sciatic axotomy

Right sciatic nerves of 3-month-old WT mice were exposed and a 5-mm segment of the nerve was removed surgically. The wound was closed with silk sutures. The Gastroctrocnemius muscle was collected for H&E staining 2 weeks after the axotomy.

Myofiber damage assay

After mice were sacrificed by cervical dislocation, FDB muscles were surgically removed to be digested in a Tyrode's solution containing type I collagenase (2 mg/ml; Sigma) at 37 °C for 60 min. After re-suspension in the Tyrode's solution, single FDB fibers were mounted on

a glass bottom chamber in Tyrode's or zero Ca^{2+} solution in the presence of 2.5 μM green-colored FM1–43 dye (Molecular Probes). To induce damage to the muscle fibers, a selected region (5 μm × 5 μm) of the plasma membrane was irradiated for 5 s with a two-photon laser (laser power 3700 at wavelength 820 nm) in a Leica Fluoview 300 confocal microscope system. Images were captured at 10-s intervals. For every image taken, the fluorescence intensity at the site of the damage was measured with ImageJ software. Fibers that had defective membrane resealing showed dye accumulation at the injury sites throughout the time course of the experiment, whereas for resealed fibers, dye influx stopped typically within 1 min.

Microelectrode penetration damage

C2C12 myoblasts or primary myoblasts were allowed to differentiate into myotubes for 3–5 days before use. Microelectrodes (borosilicate glass capillaries; World Precision Instruments, Sarasota, FL, USA) were connected to a 3-axis micromanipulator (MHH-103 Narishige International, Tokyo, Japan) to precisely control the penetration of the cell membrane in the presence of 2.5 μM red-colored FM4–64 dye (Molecular Probes). After a microelectrode was gently attached to a myotube, a further displacement of ~2 μm was considered penetration. Images were taken on an Olympus microscope equipped with a QIClick digital CCD Camera (QImaging, Surrey, BC, Canada). Live imaging of myoblasts was performed on a heated stage with the spinning disk confocal imaging system described above. Microelectrodes attached to the 3-axis micromanipulator MP-285 (Sutter Instruments, Novato, CA, USA) were used to induce penetration.

Evans Blue dye uptake

Evans blue dye (1%; 10 ml per kg body weight; Sigma) was injected into the intraperitoneal space of 1-month-old mice 8–16 h before tissue collection. Dissected Gastroctrocnemius muscles were frozen for cryosectioning.

Flow cytometry PI staining

His-tagged SLO (carrying a cysteine deletion that eliminates the need for thiol activation[26]) was provided by R. Tweeten (University of Oklahoma, Norman, OK) and purified using Ni-nitrilo-triacetic acid (NTA) agarose resin (Qiagen) in BL21 *Ecoli* expression system. The protein concentration was measured by using the Bradford assay, and stored at −80 °C until use. For each experiment, about 2×10^6 cells were trypsinized, washed with Tyrode's solution, and incubated with SLO (2–5 μg/ml) for 10 min at 37°C. Titration of SLO was performed to determine the minimum concentration required for cell permeabilization in 0 Ca^{2+} and the maximum concentration not causing significant cell loss. SLO-treated cells were then stained with 200 μg/ml propidium iodide (PI; Sigma-Aldrich) for 5 min and analyzed by FACS Flow Cytometry (iCyt Synergy; Sony). More than 10, 000 cells were used for each condition. Data were analyzed using WinList 3D software (Verity Software House).

Lysosomal enzyme release/activity

Upon SLO treatment for 15 min, the conditioned culture medium was collected for acid phosphatase (AP) and acid sphingomyelinase (aSMase) activity measurement using an AP colorimetric assay kit (Sigma) and an acid sphingomyelinase activity assay Kit (Echelon Biosciences), respectively.

Lamp1 surface staining

C2C12 were incubated with 500–800 ng/mL SLO (a concentration that causes no significant PI staining) at 37°C for 30 min. Cells were stained with PI, re-suspended in 1% BSA with anti-mouse Lamp1 (1D4B) antibody on ice for 45 min, and fixed in 2% PFA for 30 min, and were finally incubated with Alexa-488 conjugated anti-rat secondary antibody (Invitrogen) at room temperature for 1h. After re-suspension in 0.5 ml PBS, cells were analyzed on a FACS Flow Cytometer (MoFlo Astrios, Beckman Coulter). At least 10,000 cells per experiment were analyzed for the forward angle scatter, the right angle scatter, and the fluorescence intensity.

PHluorin TIRF imaging

TIRF imaging was performed at 37°C using a VisiTech Infinfity 3 array-scanning confocal microscope (VisiTech International Ltd.; Sunderland, United Kingdom) equipped with a 100× APO TIRF objective oil-immersion (Nikon, NA 1.49). MetaMorph v7.71 image acquisition software was used to process the data.

Electron microcopy analysis

For electron microcopy analysis, animals were perfused with 4% PFA and 2.5% glutaraldehyde in PBS. Muscles were surgically removed with intact tendons. Samples were prepared with standard embedding and sectioning procedures.

AAV generation and infection

CAG promoter-driven AAV1/2-GFP-ML1 virus was generated by the Gene Transfer Vector Core of the University of Iowa. Virus injection was performed on one side of the Gastroctrocnemius muscle of 1-month-old ML1 KO or 10-day-old mdx mice. The other side of the Gastroctrocnemius muscle was used as the contralateral control. Injected and noninjected contralateral leg muscles were examined after 4 weeks.

Data analysis

Data are presented as the mean ± s.e.m. Statistical comparisons were performed with analysis of variance (ANOVA). A P value < 0.05 was considered statistically significant.

Supplementary Material

Refer to Web version on PubMed Central for supplementary material.

Acknowledgements

This work was supported by NIH grants (NS062792, MH096595, and AR060837 to H.X; HL116546 and AR064241 to R.H.). We are grateful to Dr. Susan Slaugenhaupt for the ML1 KO mice, Dr. Loren Looger for the GCaMP3 construct, Robert Edwards for the Vamp7-pHluorin construct, the Center for Live-imaging at the University of Michigan for the help on TIRF Imaging, and Richard Hume and Mohammad Akaaboune for comments on the manuscript. We appreciate the encouragement and helpful comments of other members of the Xu laboratory.

References

1. Clarke MS, Khakee R, McNeil PL. Loss of cytoplasmic basic fibroblast growth factor from physiologically wounded myofibers of normal and dystrophic muscle. J Cell Sci. 1993; 106(Pt 1): 121–133. [PubMed: 8270618]
2. McNeil PL, Khakee R. Disruptions of muscle fiber plasma membranes. Role in exercise-induced damage. Am J Pathol. 1992; 140:1097–1109. [PubMed: 1374591]
3. Davies KE, Nowak KJ. Molecular mechanisms of muscular dystrophies: old and new players. Nat Rev Mol Cell Biol. 2006; 7:762–773. [PubMed: 16971897]
4. Rahimov F, Kunkel LM. The cell biology of disease: cellular and molecular mechanisms underlying muscular dystrophy. J Cell Biol. 2013; 201:499–510. [PubMed: 23671309]
5. Bansal D, et al. Defective membrane repair in dysferlin-deficient muscular dystrophy. Nature. 2003; 423:168–172. [PubMed: 12736685]
6. Chakrabarti S, et al. Impaired membrane resealing and autoimmune myositis in synaptotagmin VII-deficient mice. J Cell Biol. 2003; 162:543–549. [PubMed: 12925704]
7. Barresi R, et al. LARGE can functionally bypass alpha-dystroglycan glycosylation defects in distinct congenital muscular dystrophies. Nat Med. 2004; 10:696–703. [PubMed: 15184894]
8. McNeil P. Membrane repair redux: redox of MG53. Nat Cell Biol. 2009; 11:7–9. [PubMed: 19122591]
9. Cai C, et al. MG53 nucleates assembly of cell membrane repair machinery. Nat Cell Biol. 2009; 11:56–64. [PubMed: 19043407]
10. Sun M, et al. Mucolipidosis type IV is caused by mutations in a gene encoding a novel transient receptor potential channel. Hum Mol Genet. 2000; 9:2471–2478. [PubMed: 11030752]
11. Venugopal B, et al. Neurologic, gastric, and opthalmologic pathologies in a murine model of mucolipidosis type IV. Am J Hum Genet. 2007; 81:1070–1083. [PubMed: 17924347]
12. Dong XP, et al. The type IV mucolipidosis-associated protein TRPML1 is an endolysosomal iron release channel. Nature. 2008; 455:992–996. [PubMed: 18794901]
13. Shen D, et al. Lipid storage disorders block lysosomal trafficking by inhibiting a TRP channel and lysosomal calcium release. Nat Commun. 2012; 3:731. [PubMed: 22415822]
14. Samie M, et al. A TRP Channel in the Lysosome Regulates Large Particle Phagocytosis via Focal Exocytosis. Dev Cell. 2013; 26:511–524. [PubMed: 23993788]
15. de Figueiredo P, Brown WJ. A role for calmodulin in organelle membrane tubulation. Mol Biol Cell. 1995; 6:871–887. [PubMed: 7579700]
16. Straub V, Rafael JA, Chamberlain JS, Campbell KP. Animal models for muscular dystrophy show different patterns of sarcolemmal disruption. J Cell Biol. 1997; 139:375–385. [PubMed: 9334342]
17. Weitz R, et al. Muscle involvement in mucolipidosis IV. Brain Dev. 1990; 12:524–528. [PubMed: 2288386]
18. Zlotogora J, Ben Ezra D, Livni N, Ashkenazi A, Cohen T. A muscle disorder as presenting symptom in a child with mucolipidosis IV. Neuropediatrics. 1983; 14:104–105. [PubMed: 6877526]
19. Venugopal B, et al. Chaperone-mediated autophagy is defective in mucolipidosis type IV. J Cell Physiol. 2009; 219:344–353. [PubMed: 19117012]
20. Abe A, et al. Reduction of globotriaosylceramide in Fabry disease mice by substrate deprivation. J Clin Invest. 2000; 105:1563–1571. [PubMed: 10841515]

21. Campbell KP. Three muscular dystrophies: loss of cytoskeleton-extracellular matrix linkage. Cell. 1995; 80:675–679. [PubMed: 7889563]
22. Cai C, et al. Membrane repair defects in muscular dystrophy are linked to altered interaction between MG53, caveolin-3, and dysferlin. J Biol Chem. 2009; 284:15894–15902. [PubMed: 19380584]
23. Bansal D, Campbell KP. Dysferlin and the plasma membrane repair in muscular dystrophy. Trends Cell Biol. 2004; 14:206–213. [PubMed: 15066638]
24. Weisleder N, et al. Recombinant MG53 protein modulates therapeutic cell membrane repair in treatment of muscular dystrophy. Sci Transl Med. 2012; 4:139ra185.
25. Samie M, et al. A TRP Channel in the Lysosome Regulates Large Particle Phagocytosis via Focal Exocytosis. Dev Cell. 2013
26. Idone V, et al. Repair of injured plasma membrane by rapid Ca2+-dependent endocytosis. J Cell Biol. 2008; 180:905–914. [PubMed: 18316410]
27. Hua Z, et al. v-SNARE composition distinguishes synaptic vesicle pools. Neuron. 2011; 71:474–487. [PubMed: 21835344]
28. Reddy A, Caler EV, Andrews NW. Plasma membrane repair is mediated by Ca(2+)-regulated exocytosis of lysosomes. Cell. 2001; 106:157–169. [PubMed: 11511344]
29. Corrotte M, et al. Caveolae internalization repairs wounded cells and muscle fibers. Elife. 2013; 2:e00926. [PubMed: 24052812]
30. Jimenez AJ, et al. ESCRT machinery is required for plasma membrane repair. Science. 2014; 343:1247136. [PubMed: 24482116]
31. Demonbreun AR, et al. Impaired muscle growth and response to insulin-like growth factor 1 in dysferlin-mediated muscular dystrophy. Hum Mol Genet. 2011; 20:779–789. [PubMed: 21127009]

Method References

32. Bolsover FE, Murphy E, Cipolotti L, Werring DJ, Lachmann RH. Cognitive dysfunction and depression in Fabry disease: a systematic review. J Inherit Metab Dis. 2013
33. Springer ML, Rando TA, Blau HM. Gene delivery to muscle. Curr Protoc Hum Genet. 2002; Chapter 13(Unit13):14.
34. Dong XP, et al. PI(3,5)P(2) Controls Membrane Traffic by Direct Activation of Mucolipin Ca Release Channels in the Endolysosome. Nat Commun. 2010; 1
35. Wang X, et al. TPC proteins are phosphoinositide-activated sodium-selective ion channels in endosomes and lysosomes. Cell. 2012; 151:372–383. [PubMed: 23063126]
36. Brooke MH, Kaiser KK. Muscle fiber types: how many and what kind? Arch Neurol. 1970; 23:369–379. [PubMed: 4248905]

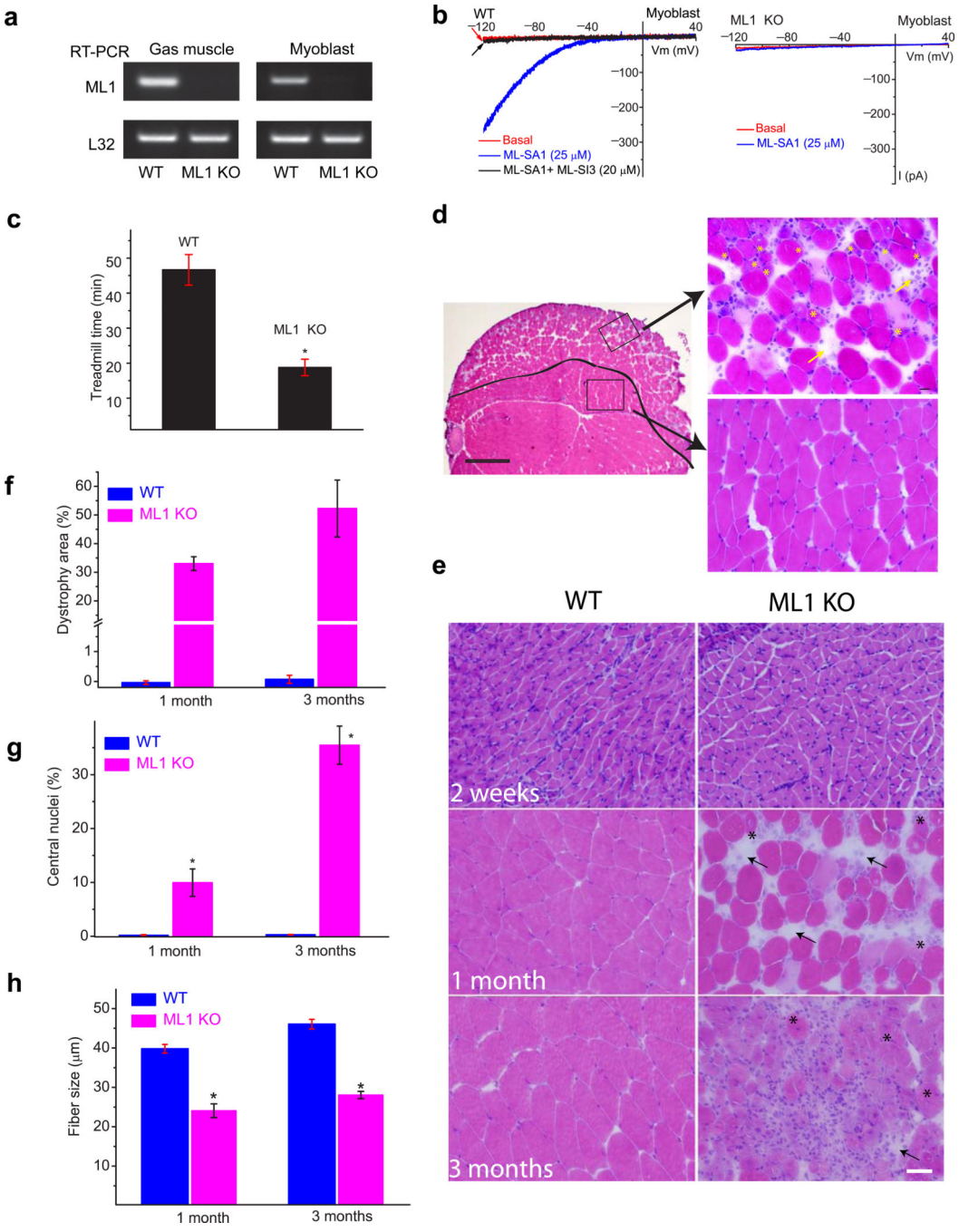

Figure 1. ML1-null mice develop early-onset progressive MD

(a) Reverse transcription-PCR analysis of WT and TRPML1 (ML1) KO Gastroc muscle and primary cultured myoblasts with a primer pair targeting the deleted region (exons 3, 4, and 5) of the *TRPML1* gene[11]. The housekeeping gene *L32* served as a loading control. **(b)** ML-SA1 (25 μM) activated endogenous whole-endolysosome ML1-like currents (I_{ML1}) in WT but not ML1 KO myoblasts. ML-SA1-activated currents were inhibited by ML-SI3 (20 μM). Currents were stimulated by using a ramp voltage protocol from −120 to +40 mV. **(c)** One-month-old ML1-null mice exhibited a shorter running time in a treadmill test compared with

WT controls. Animals were trained to run on a 15° downhill treadmill at a speed of 20 m/min. *n* = 5 animals each. **(d)** H&E staining of a Gastroc muscle section from a 1-month-old ML1 KO mouse. Scale bar = 400 μm. The black line indicates the boundary between the "dystrophic" region at the periphery and the "normal" region in the center. The representative images on the right are from the boxed areas (left) and show the centrally nucleated fibers (indicated with *) and fibrosis (arrows). Scale bar = 20 μm. **(e)** H&E staining of Gastroc muscle sections from ML1 KO mice at 2 weeks, and 1 and 3 months of age. Scale bar = 20 μm. **(f)** The percentage of the dystrophic area in ML1 KO (pink) and WT (blue) muscle. **(g)** The percentage of centrally nucleated fibers increased with age in ML1 KO. **(h)** The diameters of muscle fibers were substantially smaller in ML1 KO. For panels **f**, **g**, **h**, *n* = 3 animals for each condition. Data are presented as the mean ± s.e.m.

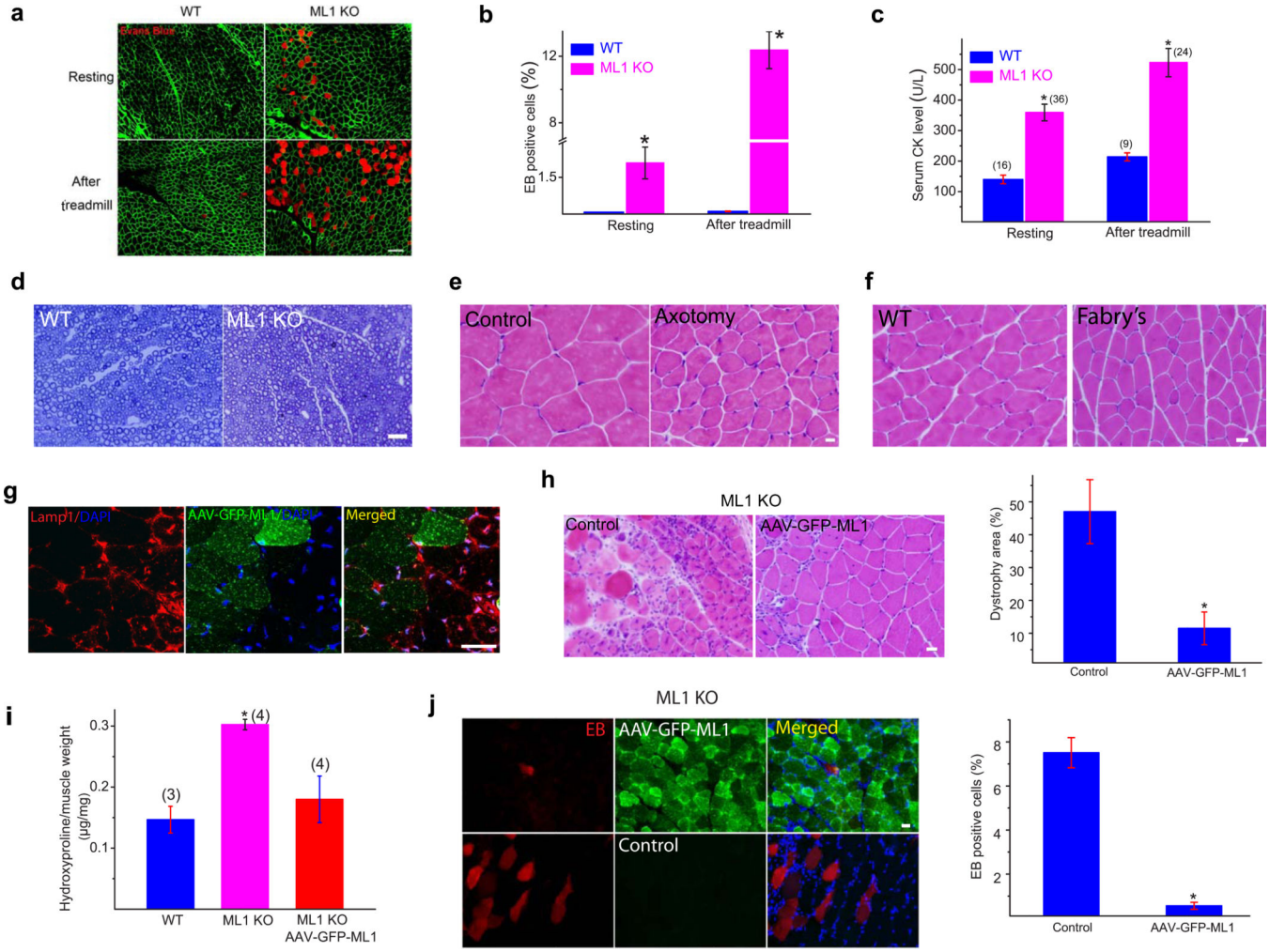

Figure 2. MD and muscle membrane damage of ML1 KO mice are not caused by neural degeneration and can be rescued by muscle expression of ML1

(a) Evans blue (EB) dye staining in WT and ML1 KO Gastroc muscles either at rest or after a 30-min treadmill test at the speed of 12 meter/min. The immuostaining of α-DG was used to label the sarcolemma. Scale bar = 40 μm. **(b)** The percentage of EB-positive muscle fibers in WT and ML1 KO mice. *n* = 3 animals for each condition. **(c)** Serum CK levels in WT and ML1 KO mice, either before or after treadmill exercise. The number of animals for each condition is indicated in the parentheses. **(d)** Lack of obvious myelination defects in the sciatic nerve of 1-month-old ML1 KO mice. **(e)** Sciatic axotomy induced atrophy of WT Gastroc muscle. **(f)** Atrophic Gastroc muscle of 4-month-old Fabry's mice. Scale bar = 20 μm. **(g)** AAV-GFP-ML1-infection reduced Lamp1 elevation in ML1-null muscle cells compared with neighboring noninfected controls. Scale bar = 40 μm. **(h)** The effect of AAV-GFP-ML1 infection on the dystrophic phenotype in ML1 KO muscles; H&E staining revealed deceased levels of necrosis and fibrosis. The right panel shows a decrease in the percentage of the dystrophic area in ML1-null muscle. *n* = 4 animals for each condition. **(i)** AAV-GFPML1 infection on collagen content in ML1 KO muscle. The content of hydroxyproline, a marker for collagen content, was measured in Gastroc skeletal muscle

from 3-month-old WT and ML1 KO mice. **(g)** The effect of AAV-GFP-ML1 infection on EB uptake in ML1-null muscle. *n* = 3 animals for each condition. Data are presented as the mean ± s.e.m. Scale bars = 10 μm for panels **d**, **e**, **h**, and **i**.

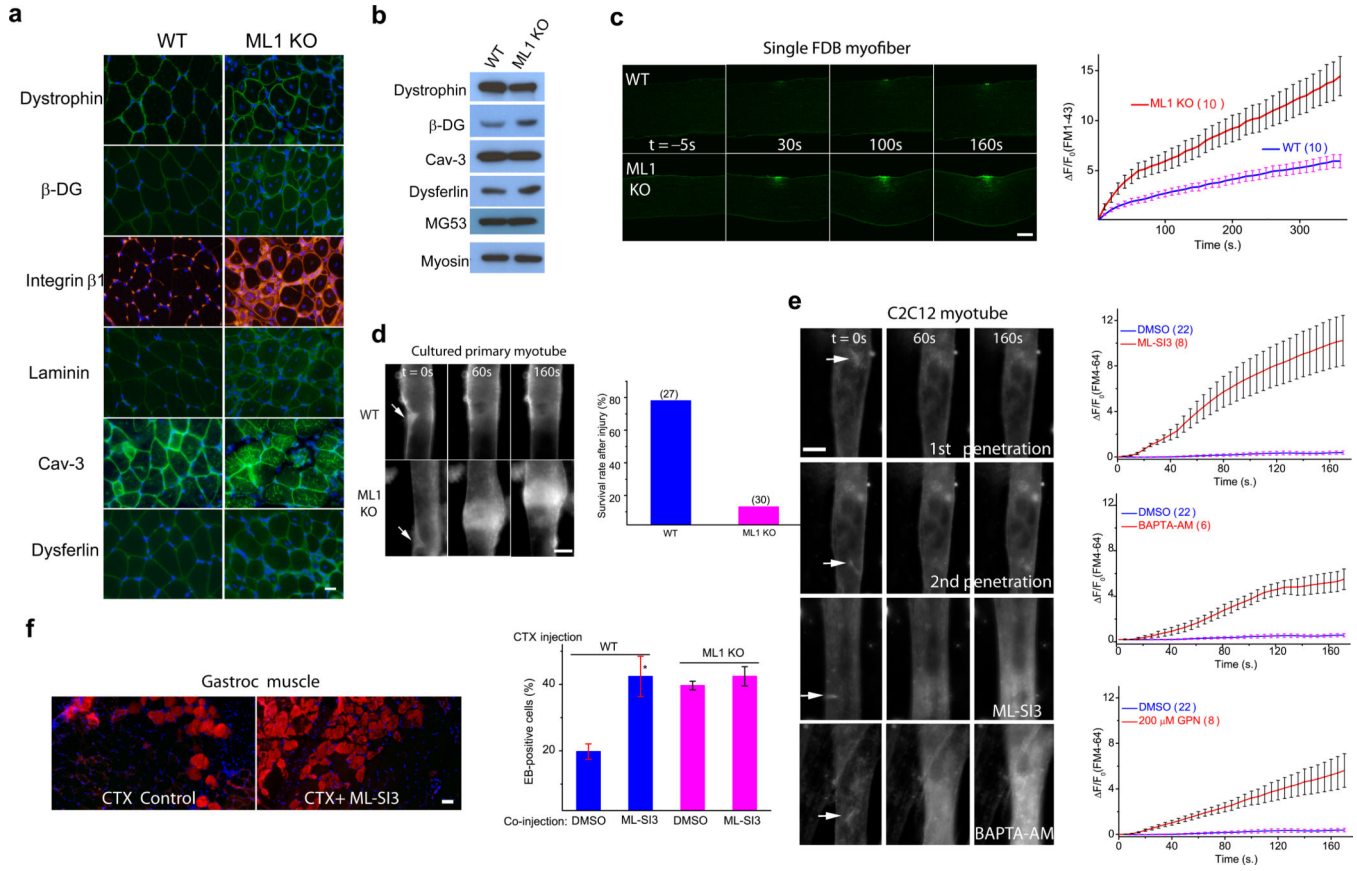

Figure 3. Defective membrane repair capacity in ML1 KO muscle

(a) Immunofluorescence of dystrophin, β-dystroglycan (β-DG), integrin β1, laminin, caveolin-3 (Cav-3), and dysferlin in ML1-null Gastroc muscle. Scale bar = 10 μm. **(b)** Western blotting analysis of the DGC components, Cav-3, dysferlin, and MG53 in ML1 KO mice. Myosin served as a loading control. **(c)** A membrane repair assay performed on single FDB muscle fibers isolated from WT and ML1 KO mice. Membrane damage was induced with a two-photon laser at t = 0 s. Scale bar = 10 μm. The right panel shows the time-dependent changes (ΔF) in FM1–43 fluorescence intensity normalized to the basal fluorescence (F_0) for WT (blue) and ML1 KO (red) fibers. **(d)** Representative images of *in vitro* differentiated myotubes in response to mechanical damage elicited by a microelectrode (arrows). The lower panel shows the percentage of "surviving" myotubes in response to microelectrode penetration. The experiments were performed in the presence of extracellular Ca^{2+}, and defective membrane resealing led to excessive Ca^{2+} influx that triggered prolonged muscle contraction. The "surviving" cells are those without prolonged contraction. Scale bar = 50 μm. **(e)** Responses of C2C12-derived myotubes to microelectrode penetration in Tyrode's solution (2 mM Ca^{2+}) in the presence of DMSO (0.1%; 1st and 2nd penetration), ML-SI3 (20 μM), BAPTA-AM (20 μM), and GPN (200 μM). The right panels show the time course of FM4–64 accumulation ($\Delta F/F_0$) at injury sites following microelectrode penetration. Scale bar = 50 μm. Note that the same set of DMSO control data was compared with all groups of drug treatment. **(f)** The effect of ML-SI3, a TRPML-specific synthetic inhibitor, on EB dye uptake in WT Gastroc muscles injected with

the cardiotoxin VII4 (CTX), a cytolytic toxin that disrupts cell membrane in living animals[24]. The lower panel shows that intramuscular coinjection of ML-SI3 with CTX on EB dye uptake in WT and ML1 KO muscle. Scale bar = 10 μm. Data are presented as the mean ± s.e.m, n = 3 animals for each condition.

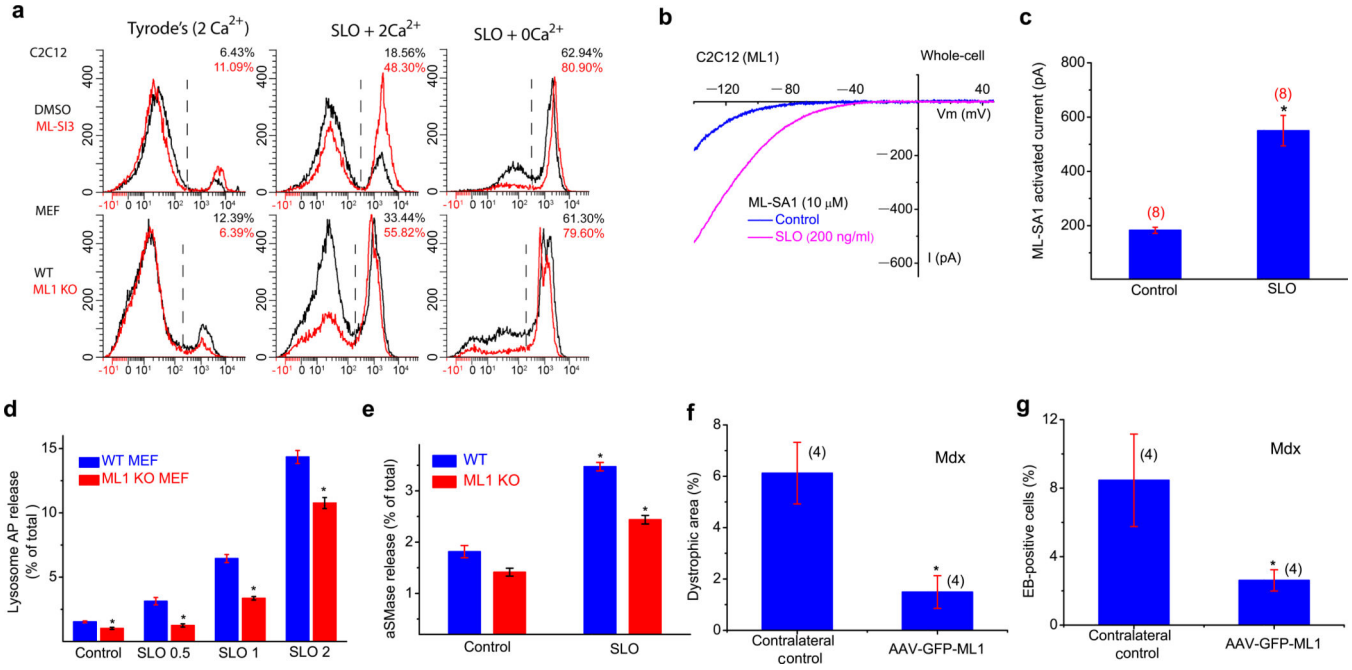

Figure 4. An essential role of ML1 in lysosomal exocytosis, membrane repair, and protection of muscle damage *in vivo*

(**a**) C2C12 and MEF cells were treated with pore-forming toxin streptolysin O (SLO; 2–5 μg/ml), and stained with PI, a marker for membrane damage. FACS quantification of PI staining was performed in cells with or without SLO or external Ca^{2+} (2 mM). (**b, c**) SLO (0.2 μg/ml) treatment increased whole-cell I_{ML1} in C2C12 cells transfected with GFP-ML1. **d,** SLO (0.5, 1 and 2 μg/ml for 15 min) treatment on the release of lysosomal acid phosphatase (AP; determined using an AP activity colorimetric assay kit) into the culture medium in WT and ML1 KO MEFs. The data are presented as the percentage of the activity of the released *vs*. total cell-associated enzymes. **e,** SLO (0.5 μg/mL for 15 min) treatment on the release of lysosomal acid SMase (aSMase; determined using an aSMase activity assay kit) in WT and ML1 KO MEFs. (**f, g**) The effect of AAV-GFP-ML1 infection on EB uptake and dystrophic area in mdx Gastroc muscle. Data are presented as the mean ± s.e.m.